# Defining Mesh-LBP Variants for 3D Relief Patterns Classification

Claudio Tortorici[1][0000−0001−6943−2854], Naoufel Werghi[1], and Stefano Berretti[2]

[1] Khalifa University, Abu Dhabi, UAE
{Claudio.Tortorici,Naoufel.Werghi}@kustar.ac.ae
[2] University of Florence, Florence, Italy
Stefano.Berretti@unifi.it

**Abstract.** Extending the concept of texture to the geometry of a mesh manifold surface, opened the way to the idea of classifying 3D relief patterns as an emerging topic in 3D Computer Vision, with several potential applications. In this paper, we propose an original modelling solution to address this novel task. Following the recent introduction of the LBP computation framework on mesh manifolds (mesh-LBP), we first extend this framework to the different variants of 2D LBP by defining mesh-LBP variants. The compliance of these extensions with the original LBP in terms of uniformity is also investigated. Then, we propose a complete framework for relief patterns classification, which performs mesh preprocessing, multi-scale mesh-LBP extraction and descriptors classification. Experimental results on the SHREC'17 dataset show competitive performance with respect to state of the art solutions.

## 1 Introduction

The recent advancements of 3D imaging technologies resulted in a new generation of acquisition devices capable of capturing the geometry of 3D objects. High-resolution 3D static scanners as well as devices with 3D dynamic acquisition capabilities that provide a continuous flow of the 3D geometry of a scene are now available. In addition to this, the geometric and photometric information are often captured in a synchronized way. The geometric information captured by such devices represents the 3D coordinates of a set of samples of the object surface, typically in the form of a point cloud. However, directly processing point clouds is not convenient or even possible so that other representation formats have established. Depth images are one of the most commonly used imaging modality, since they permit a straightforward extension to the depth dimension of many computer vision and pattern recognition solutions developed in the literature for analyzing the photometric information in 2D images. Though the idea of extending 2D techniques is attractive, this modality loses the full 3D geometry by reducing it to a 2.5D projection. Instead, the full 3D shape information of an object can be preserved and encoded in a simple, compact and flexible format by using a triangular mesh manifold. However, passing from a point cloud to a mesh manifold is not an easy problem in itself: reconstructing the real structure of the manifold surface is often difficult, especially in the case of objects with complex topology or when multiple scans of the same object must be merged together [27].

Using mesh manifolds as inputs, several studies addressed the problem of retrieving/classifying 3D shapes based on their similarities [27]. In most of the cases, synthetic models generated by ad-hoc softwares have been used, while reconstructed meshes have been considered more rarely. An even less investigated but emerging problem, which is of interest for its potential application in several contexts, is that of classifying 3D relief patterns. A peculiar characteristic of patterns is the fact their style does not depend by the overall structure of the shape, rather it identifies parts and local properties that are independent of the global shape. In particular, relieves of interest are those characterized by some form of regularity and repeatability across the surface so that they can be regarded as the 3D geometric equivalent of textures in 2D images. Examples are knitted fabrics, artworks patterns, artists styles or natural structures like tree barks [23], rock types or engravings [39], etc.

A recent trend, motivated by outstanding results in several challenging contexts, applies deep convolutional neural network architectures to solve a number of detection, recognition and classification problems in 2D still images or videos [14,17,26]. The application of such deep learning tools is facilitated by the grid structure of images and the access to large repositories of training data. Less obvious appears the extension of such framework to geometric contexts, such as graphs, matrix manifolds, or meshes [6]. Though some results in this direction do exist, they are not yet as competitive as 3D "classic" solutions [12] and consolidated as in 2D. The need for large training dataset remains also an obstacle in 3D applications due to the difficulty of acquiring very large repositories of 3D scans [29]. The recent PointNet deep learning solution proposed by Charles et al. [7], while addresses effectively object classification in point cloud format, is suited for volumetric objects rather than shape texture variations on the manifold.

On another side, LBP has been one of the most simple and widely spread local texture descriptor in 2D and 2.5D. LBP has been proposed as texture descriptor for 2D still images for the first time by Ojala et al. [22]. Thanks to its simplicity and discriminative power, LBP has been successfully implemented for Visual Inspection [18], Remote Sensing [9], Motion Analysis [30], Face Recognition [1,2] and Expression Recognition [24] in both 2D and 2.5D supports. However, its application to mesh manifolds could not be achieved till a mesh-version was introduced by Werghi et al. [36,34,35,37].

Based on the above considerations, in this paper, we propose a novel solution for 3D relief patterns classification, which relies on the extension of LBP and its variants to mesh manifolds. In doing so, as first contribution of our work, we define the mesh-LBP variants as counterparts of LBP variants on the triangular mesh manifold support, and assess their descriptive capabilities. Then, as second contribution, we propose an original modeling approach that uses mesh-LBP variants in the task of relieves classification. This is obtained by presenting a complete framework that includes a suitable preprocessing of the mesh, multi-scale extraction of mesh-LBP descriptors, and descriptors classification using SVM.

## 2 Related Work

The problem of relief pattern classification is of quite new definition. Therefore, most of the works that we summarize in the following have been presented and participated to the SHREC'17 contest, track on "Retrieval of surfaces with similar relief patterns" [5].

One of the first work addressing the problem of effectively describing 3D relief patterns is due to Werghi et al. [31,32]. In their work, mesh-LBP was proposed as a extension of LBP to mesh manifolds. They also showed the applicability of this approach for geometric texture retrieval for a small set of prototype meshes.

In order to capture texture features of object surface, Tatsuma and Aono [5] estimated statistics of local features extracted from the depth-buffer image as a shape descriptor. To emphasize the texture of object surface, they converted the depth-buffer image into the LBP image. For feature detection and description from the LBP image (LBPI), the KAZE features [3] was employed.

Limberger and Wilson [5] proposed a curvature-based Laplace Beltrami operator (KLBO) to describe the relief patterns of surfaces. After computing the eigendecomposition of the KLBO, the Improved Wave Kernel signature (IWKS) [16] was computed and encoded using two different encoding schemes: the Fisher Vector (FV) or the Super Vector (SV). Lastly, differences between encodings were computed using Euclidean distance, after reducing feature dimensionality by computing PCA.

Siprian and Bustos [5] applied the Signature Quadratic Form Distance (SQFD) [4] along with intrinsic spectral descriptors for relief retrieval. On the one hand, the SQFD distance is used as a suitable and effective alternative to compare 3D objects represented as a collection of local features [25]. On the other hand, spectral features have proven to be robust against several transformations, while keeping discriminative geometric information. This proposal combined these two methods in order to represent and assess the similarity between relief patterns.

In [5], Velasco-Forero and Fehri, proposed an image covariance descriptor from morphological transformation of local curvature estimation for a given 3D mesh (CMC). Four main components were used to compute this descriptor: (1) The local principal curvatures and the Gaussian curvature were first computed; (2) Curvature values on the 3D surface were projected to a flat 2D surface. Accordingly, the boundary of the mesh, i.e., the set of vertices that are only referenced by a single triangle in the mesh was found. Three curvature images for the boundary were then derived using SVM for solving a regression problem on the boundary points; (3) Morphology operators were then applied to the curvature images, with 32 transformations with a final total of 96 images; (4) The covariance matrix of 96 images was computed, thus producing a descriptor as a square matrix of size $96 \times 96$. The similarity between two meshes was calculated via their representation as covariance matrices.

Sun et al. [5] developed on the idea of modelling convex/concave properties and local geometrical features by the interior dihedral angle of each edge of the mesh. In doing so, they proposed a statistical feature called Interior Dihedral Angle Histogram (IDAH). Firstly, they calculated all the interior dihedral angles of the model surface. Then, the distribution histogram was calculated in different intervals. Finally, they adopted the Manhattan distance between histograms to describe the model similarity. Also, the authors converted the model into a "geometry image". The 3D model is parametrized

on a spherical domain and then mapped onto an octahedron, which is then cut on its edges obtaining a flat and regular geometry image. HOG features are extracted from the geometry image (GI HOG).

Masoumi et al. [5] used a Geodesic Multi-Resolution (GMR) descriptor [19] by incorporating the vertex area into the definition of spectral graph wavelet [15] in a bid to capture more geometric information and, hence, further improve its discriminative ability. Moreover, Mexican hat wavelet has been utilized as a generating kernel, which considers all frequencies equally-important overall as opposed to the cubic spline kernel [15].

## 3 Background on LBP and LBP Variants

On its first definition, LBP generates a binary sequence for each image pixel (from now on referred as *central pixel*) analyzing its neighborhood inside a $3 \times 3$ window. According to (1), each neighbor pixel value ($n_i$) is compared with the central one ($n_c$), assigning 1 if the value is greater or equal, and 0 otherwise:

$$\textit{LBP}(n_c) = \sum_{i=0}^{N-1} s(n_i - n_c) \cdot 2^i \ , \tag{1}$$

where $s(x)$ is the step function. Then, the binary value is multiplied by the power of two with respect to the given pixel position. Later on, in [21] a multi-scale and rotation invariant LBP version was presented.

One of the firstly proposed LBP variant is the *Median Binary Pattern* (MBP) [10]. Compared to standard LBP that uses $n_c$ as threshold, the simple local median among all the neighbor values is used to reduce the error caused by noise. MBP is, therefore, a 9 bits pattern since it considers the central pixel like its surroundings.

In [40], a combination of binary patterns is used for Face Recognition. *Completed Local Binary Pattern* (CLBP) considers not only the sign of $d_i = n_i - n_c$ (CLBP-S in (1)), but also its magnitude $|d_i|$ (CLBP-M) and central pixel intensity (CLBP-C), adding more discriminant power.
CLBP-S/M/C are then combined in different configurations, such as histograms concatenation or multi-dimensional histogram computation.

A new branch of LBP variants expanded after the first presentation of a *Center-Symmetric LBP*. CS-LBP compares center-symmetric pair of pixels ignoring the central pixel value [11]. This technique halves the number of comparisons, leading to faster computation and smaller descriptor size. Without $n_c$, CS-LBP requires a threshold $\tau$:

$$\textit{CS-LBP}_{R,N}(\tau) = \sum_{i=0}^{(N/2)-1} s\left(n_i - n_{i+(N/2)}\right) \cdot 2^i \ , \quad s(x) = \begin{cases} 1 \ x \geq \tau \\ 0 \ x < \tau \end{cases} \tag{2}$$

being $n_i$ and $n_{i+(N/2)}$ the pairs of center-symmetric values, while $s(x)$ is the step function.

To overcome the limitation of the threshold, in [38] an *Improved CS-LBP* (ICS-LBP) has been designed. Similarly to (2), ICS-LBP compares center symmetric couples of pixels using the central pixel value as discriminant.

Otherwise, it is possible to replace $n_c$ with the mean $m = \frac{1}{N}\sum_{i=0}^{N-1} n_i$, to reduce noise dependency as discussed in [13].

In [8], *Centralized Binary Pattern* (CBP) takes the advantage of comparing center-symmetric couple of pixels, but it also comprehends the value of the central pixel, applying the largest weight to it. In this way, the effectiveness of the central pixel value is strengthened, and a discriminant power is added to a smaller size descriptor.

Another family of LBP variants is characterized by the use of masks on window's values. While conventional LBP encodes the values as a non-directional 1st order operator among local neighbors, in [20] a Sobel operator is applied to generate a first order derivative along $x$ and $y$ directions to characterize the image information: where $*$ is the convolution operator with the original image. Then, the gradient magnitude image $I_{gm} = \sqrt{I_x^2 + I_y^2}$ is obtained. The LBP is finally generated using (1) with $I_{gm}$ values encoding the magnitude of local variations.

## 4 Mesh-LBP Variants

Mesh-LBP is an LBP-like descriptor employed on mesh manifolds [32], particularly in 3D face recognition [36]. While the potentiality of using a real 3D support has been investigated in [37,28], the possibility to export successfully 2D LBP variants to the mesh manifold has to be addressed yet. While standard LBP compares 8 pixels belonging to a circle of a certain radius around a central pixel, mesh-LBP generates a concentric sequence of ring-like patterns around a central facet, whereby facets are ordered in a circular fashion in each ring. Mesh-LBP computation is shown in (3), whereby $r$ and $m$ are the ring number, and the number of facets per ring, respectively, $s$ is the step function, and $h$ is a scalar function on the mesh. $\alpha(k)$ is a discrete function, where $k$ represents the facet position.

$$meshLBP_m^r(f_c) = \sum_{k=0}^{m-1} s(t) \cdot \alpha(k) \qquad \text{with } \; t = h(f_k^r) - h(f_c) \tag{3}$$

Two functions were defined in the mesh-LBP, namely, $\alpha_1(k) = 1$ that sums the digits of the pattern; and $\alpha_2(k) = 2^k$ that multiplies single digit by a power of 2, as originally proposed in [22].

So far, seven mesh-LBP variants have been implemented and tested: (a) mesh-MBP, (b) mesh-CSLBP, (c) mesh-ICSLBP, (d) mesh-ICSLBP-M with central facet value replaced by the mean across the ring as threshold, (e) mesh-CBP, (f) mesh-CLBP and (g) mesh-LBP-Sobel. Considering these seven variants, the original mesh-LBP with the two functions $\alpha_1$ and $\alpha_2$, and the three scalar functions on the mesh (*Local Depth* (LD), *Mean Curvature* (H), and *Curvedness* (C)), we have a total of $8 \times 2 \times 3 = 48$ mesh-LBP variants. We can categorize these in $\alpha_1$ and $\alpha_2$ variants. Also, since the LBP is a differential operator, we can categorize the variants as first-order and second order differentiation variants, depending on the fact the scalar function on the mesh represents a raw entity (e.g., LD) or a derivative entity (e.g., H and C).

In the particular case of mesh-MBP, $\alpha_1(k)$ is meaningless because it uses a median threshold; while for mesh-CLBP, $\alpha_2(k)$ is skipped because of its pattern length (see Table 1). Therefore, the total number of variants investigated is 42.

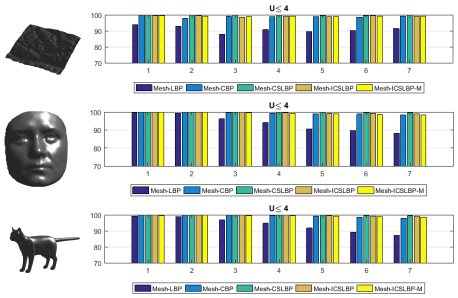


Fig. 1: Uniformity analysis performed on three sample meshes from different datasets. The histograms show the percentage of patterns with a number of $0/1$ transitions $U \leq 4$. Reported results have been obtained with the $H$ descriptor.

| Mesh-LBP variant $(U)$ | size $\alpha_1$ | size $\alpha_2$ |
|---|---|---|
| Mesh-LBP $(4)$ | 13 | 1125 |
| Mesh-MBP $(6)$ | 13 | 2973 |
| Mesh-CSLBP $(4)$ | **7** | **63** |
| Mesh-ICSLBP $(4)$ | **7** | **63** |
| Mesh-ICSLBP-M $(4)$ | **7** | **63** |
| Mesh-CBP $(4)$ | **8** | **115** |
| Mesh-CLBP $(6)$ | 26 | 380103 |

Table 1: Comparison of pattern size and histogram size for $\alpha_1(k)$ and $\alpha_2(k)$, for the different mesh-LBP variants. Uniformity applied within brackets $(U)$.

We compared the mesh-LBP variants to the standard mesh-LBP. First, we focused on the uniformity aspect of the mesh-LBP variants descriptor (see Section 4.1); then, we reported results for 3D Relief Pattern Classification (see Section 6).

### 4.1 Uniformity

In [21], evaluating the rotation invariant pattern, authors counted the number of $0/1$ transitions in the binary pattern, and evaluated their frequency of occurrence. Then, they observed that most of the pattern configurations had a number of transitions $(U)$ less than 2, So, a unique label (defined as "uniform") can be assigned to all the patterns with number of transitions above 2; that grouping method allows reducing the descriptor size, while increasing its accuracy.

The same analysis has been performed for all our mesh-LBP variants considering $R = 1, \ldots, 7$ concentric rings around the central facet, and $N = 12$ points at each ring. Since uniformity mainly depends on the pattern of the specific variant, mesh-LBP-Sobel performs exactly as standard mesh-LBP, so regarding the uniformity analysis we will refer to both of them as mesh-LBP. Although Center-Symmetric based approaches, especially mesh-CSLBP and mesh-ICSLBP, have over $70\%$ of patterns with $U \leq 2$ among all the seven rings, we choose a more conservative value $U \leq 4$. Figure 1 depicts the average percentage of uniform patterns, with $U \leq 4$ using the $H$ descriptor. As shown in the figure, four variants over six outperform the standard mesh-LBP percentage of patterns with number of transitions $U \leq 4$: they all belong between $97\% - 100\%$ even at rings 6 and 7. Mesh-CLBP and mesh-MBP, instead, reach an average above $85\%$ with $U \leq 6$ due to their pattern length and characteristics. Grouping all the patterns with $U$ greater than a predefined value, it is possible to considerably reduce the size of $\alpha_2(k)$ descriptors as shown in Table 1.

## 5 Relief Patterns Classification

In this Section, we propose to use the mesh-LBP variants for relief pattern classification. These patterns are given by geometric corrugations of the mesh with some regularity and repetition and can be regarded as the surface equivalent of textures in 2D images. Similarly to the 2D case, relief patterns (or geometric texture) are difficult to represent and classify. They may be repetitions of simple textons of any size, or spread on the whole surface. To handle such variety, we decided to represent the texture using multi-scale histograms computed on circular regions. The possibility to describe the texture with different scale factors helps to cope with different texture typology.

We used *Ordered Rings of Facet* (ORF) [33] to generate three concentric rings (Figure 2a). Such rings are sampled according to their diameter. Circular regions are then extracted around each sampled point, and mesh-LBP histogram computation is applied on the covered region. To comprise multi-scale information, the number of sampled points at each ring and the circular region size are varied. While increasing the region size, the number of points at each concentric ring decreases as shown in Figure 2b, 2c and 2d. Finally, in order to augment the histogram representation power, the multi-scale descriptors have been generated at three different locations for each training sample, while only one location is used for the test.

Such descriptors are used to feed an SVM classifier. Here, two types of classification have been used: (1) **One-vs-all** that trains one SVM for each class. In this case, positive examples come from one class, while negative examples come from all the other classes. (2) **One-vs-one** that trains $\frac{n(n-1)}{2}$ SVMs, where $n$ is the number of classes. For each SVM, positive examples come from one class, and negatives from another one.

## 6 Experimental Results and Evaluation Protocol

In Section 4, we have introduced the mesh-LBP variants and investigated their main properties in a set of tests that proved their relevance with respect to the original mesh-LBP. Based on this, in the following we experiment the mesh-LBP variants in the specific task of relief patterns classification. In doing so, we use a dataset introduced for an open competition that allows us to compare with state of the art solutions.

Recently, a new database has been released for the SHREC'17 contest track on "*Retrieval of surfaces with similar relief patterns*" [5]. The database is composed by different patches of various textiles, each acquired in different poses and deformed shape situations (a total of 180 models referred as *original* surfaces). For each scan, three processing operations, designed to alter the mesh connectivity, have been applied to obtain, respectively, meshes with 5K, 10K and 15K vertices. The database has a total of 720 samples.

The SHREC'17 competition protocol required the participants to submit a $720 \times 720$ matrix of mutual distances between all the database samples. Organizers elaborated such matrices and evaluated them using several criteria such as Nearest Neighbor (NN), First Tier (FT), Second Tier (ST) and other distances differentiating between the full dataset (720 samples) and the dataset composed by the 180 original meshes. Also, confusion matrices obtained from the NN classification were presented from the best results of each participant.

Table 2: Comparison with the results of the SHREC'17 competition as reported in [5]. Scores refer to the full dataset using Nearest Neighbor (NN) classification. We report generically "Mesh-LBP Variants" since they all score the same.

| | **Classification Method** | **NN** |
|---|---|---|
| [5] | CH | 19.60% |
| | LBPI | 82.80% |
| | IDAH-1 | 39.00% |
| | IDAH-2 | 30.60% |
| | GI HOG | 68.60% |
| | SQFD-SIHKS | 16.80% |
| | SQFD-HKS | 53.60% |
| | SQFD-WKS | 51.00% |
| | CMC-1 | 71.80% |
| | CMC-2 | 76.30% |
| | CMC-3 | 64.70% |
| | **KLBO-FV-IWKS** | **98.60%** |
| | KLBO-SV-IWKS | 97.80% |
| | GMR | 7.90% |
| **Mesh-LBP Variants** | | **99.77%** |

Fig. 2: The multi-scale regions used to describe a mesh sample are reported: 2a concentric rings, where the sampling points are located; 2b-2d multi-scale region extraction.

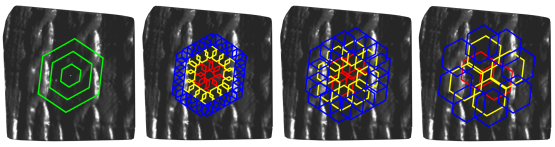

(a) (b) (c) (d)

Table 3: 5-folds cross validation SVM results. Only Center-Symmetric based variants/descriptors are reported for efficiency reasons.

| Descriptor Combination | $\alpha_2$ | |
|---|---|---|
| | **One-vs-All** | **One-vs-One** |
| Mesh-CSLBP-H | 97.73% | 97.60% |
| Mesh-CSLBP-C | 97.07% | 97.07% |
| Mesh-CSLBP-LD | 94.93% | 95.20% |
| Mesh-ICSLBP-H | 93.60% | 93.73% |
| Mesh-ICSLBP-C | 95.20% | 94.93% |
| Mesh-ICSLBP-LD | 98.00% | 97.87% |
| Mesh-ICSLBP-M-H | 95.47% | 95.47% |
| Mesh-ICSLBP-M-C | 96.40% | 96.53% |
| Mesh-ICSLBP-M-LD | 96.80% | 97.07% |
| Mesh-CBP-H | 97.20% | 96.93% |
| Mesh-CBP-C | 96.67% | 96.93% |
| **Mesh-CBP-LD** | **98.53%** | **98.53%** |

### 6.1 Results and Comparative Evaluation

In our tests, we performed the same experiment of the SHREC'17 competition with our representation based on mesh-LBP variants comparing our results with those obtained by the SHREC participants. We performed the experimentation on all the 7 mesh-LBP variants, plus the original mesh-LBP. Each variant has been computed using Mean curvature (H), Curvedness (C) and Local Depth (LD) in both their variants $\alpha_1$ and $\alpha_2$ as described in Section 4.

The database is split into 5 folds: 4 used for training, and 1 for testing. The classification is repeated five times in order to use all the 5 folds as test samples.

Globally, the methods presented in [5] perform quite poorly. In Table 2, we compare the best results obtained by SHREC participants on the full database against those resulting with our method and a baseline method proposed by SHREC'17 organizers. The baseline method consist of a 128 bins histogram of the minimal curvature of the surface (CH). SHREC participants used different distances to compare their descriptors in the NN classification. We adopted the Bhattacharyya, Cosine and $\chi^2$ distances ob-

taining the same score among all the variants tested. All our variants outperform the others, overtaking even the best KLBO-FV-IWKS result.

Since such results have been obtained with NN classification, they can be biased by the inclusion of 4 meshes of the same original sample (i.e., meshes obtained by resampling the original mesh with 5K, 10K and 15K vertices). Therefore, organizers performed the same evaluation on the 180 original samples to get a better understanding of the classification capabilities of the different approaches when considering only the different samples of the same class, avoiding comparison with resampled meshes. In this evaluation, all presented methods drastically decreased their performance, getting a maximum of $63.3\%$ (CMC-2), while KLBO-FV-IWKS scored only $52.2\%$ at its best value. The aim of such experiment is to judge the method performance on practical applications, evaluating their ability in pattern retrieval: KLBO-FV-IWKS, in fact, seems to include global shape information in its classification producing such accuracy decay (from $98.6\%$ to $52.2\%$ on its best result).

We designed a method capable of measuring the class discrimination using SVM as described in Section 5. To design a fair comparison, we need to specify that the protocol implemented is not exactly the same as for the SHREC'17 competition. Indeed, it considers all the database samples, however the contribution of resampled meshes during the training phase is minimal, and does not substantially affect the class discrimination. In the hypothetic best case, three samples of the same patch would be on the training set, while one used as test; with $48$ samples per class, and our $5$-folds classification method, the three meshes would be less than $7.8\%$ of the training sample, while $5.2\%$ and $2.6\%$ if the samples in the training are two or one, respectively. As shown in Table 3, our mesh representation based on mesh-LBP variants clearly outperforms results presented in [5]. The LD descriptor scores the best among all the mesh-LBP variants except for mesh-CSLBP. Moreover, the ability to shrink the histogram size of some mesh-LBP variants (see Table 1), allowed us to gain on the SVM training performances. In fact, $\alpha_2$ descriptors show remarkable scores all between $93.60\%$ and $98.53\%$.

## 7 Discussion and Conclusion

In this paper, we extended different varieties of LBP variants to the mesh manifold, whereby we derived a total of 48 variants on the mesh by combination of different scalar functions on the mesh and binary digits weights.

Our study reveals that the mesh variants preserve the original behavior of their 2D counterparts with regard to the uniformity aspect. Also, a comparative study for geometric texture detection, has shown mesh-LBP variants capabilities to enhance further analysis tasks on mesh manifold. Referring to Table 1, four new mesh-LBP variants substantially reduced the computational cost by bringing down the histogram size to 63 and 155, as compared to the original size of 1125 in the original mesh-LBP. Our experiments reveal that such small size mesh-LBP boost the SVM training efficiency without compromising the accuracy. Comparing with the most recent state of the art works proposed for relief patterns classification, tested on the SHREC'17 data set, SVM results showed a clear improvement brought by our mesh-LBP extension approach.

## References


1. Ahonen, T., Hadid, A., Pietikäinen, M.: Face Recognition with Local Binary Patterns, pp. 469–481. Springer Berlin Heidelberg, Berlin, Heidelberg (2004), http://dx.doi.org/10.1007/978-3-540-24670-1_36
2. Ahonen, T., Hadid, A., Pietikainen, M.: Face description with local binary patterns: Application to face recognition. IEEE Trans. on Pattern Analysis and Machine Intelligence 28(12), 2037–2041 (Dec 2006)
3. Alcantarilla, P.F., Bartoli, A., Davison, A.J.: Kaze features. In: European Conf. on Computer Vision. pp. 214–227 (2012), https://doi.org/10.1007/978-3-642-33783-3_16
4. Beecks, C., Uysal, M.S., Seidl, T.: Signature quadratic form distances for content-based similarity. In: ACM Int. Conf. on Multimedia. pp. 697–700 (2009), http://doi.acm.org/10.1145/1631272.1631391
5. Biasotti, S., Thompson, E.M., Aono, M., Hamza, A.B., Bustos, B., Dong, S., Du, B., Fehri, A., Li, H., Limberger, F.A., Masoumi, M., Rezaei, M., Sipiran, I., Sun, L., Tatsuma, A., Forero, S.V., Wilson, R.C., Wu, Y., Zhang, J., Zhao, T., Fornasa, F., Giachetti, A., Velasco-Forero, S., Wilson, R.C., Wu, Y., Zhang, Y., Zhao, T., Formasa, F., Giachetti, A.: Shrec'17 Track: Retrieval of surfaces with similar relief patterns (apr 2017), https://hal.archives-ouvertes.fr/hal-01500436https://diglib.eg.org/handle/10.2312/3dor20171058
6. Bronstein, M.M., Bruna, J., LeCun, Y., Szlam, A., Vandergheynst, P.: Geometric deep learning: Going beyond euclidean data. IEEE Signal Processing Magazine 34(4), 18–42 (July 2017)
7. Charles, R.Q., Hao, S., amd J.G. Leonidas, M.K.: Pointnet: Deep learning on point sets for 3d classification and segmentation. In: IEEE International Conference on Computer Vision and Pattern Recognition. IEEE (2017)
8. Fu, X., Wei, W.: Centralized Binary Patterns Embedded with Image Euclidean Distance for Facial Expression Recognition. In: 2008 Fourth International Conference on Natural Computation. vol. 4, pp. 115–119. IEEE (2008), http://ieeexplore.ieee.org/document/4667260/
9. Guo, D., Atluri, V., Adam, N.: Texture-based remote-sensing image segmentation. In: 2005 IEEE International Conference on Multimedia and Expo. pp. 1472–1475 (July 2005)
10. Hafiane, A., Seetharaman, G., Palaniappan, K., Zavidovique, B.: Rotationally Invariant Hashing of Median Binary Patterns for Texture Classification. In: Image Analysis and Recognition, pp. 619–629. Springer Berlin Heidelberg, Berlin, Heidelberg (2008), http://link.springer.com/10.1007/978-3-540-69812-8{_}61
11. Heikkilä, M., Pietikäinen, M., Schmid, C.: Description of interest regions with local binary patterns. Pattern Recognition 42(3), 425–436 (mar 2009), http://linkinghub.elsevier.com/retrieve/pii/S0031320308003282
12. Ioannidou, A., Chatzilari, E., Nikolopoulos, S., Kompatsiaris, I.: Deep learning advances in computer vision with 3d data: A survey. ACM Computer Survey 50(2), 20:1–20:38 (Apr 2017), http://doi.acm.org/10.1145/3042064
13. Junding, S., Shisong, Z., Xiaosheng, W.: Image retrieval based on an improved CS-LBP descriptor. 2010 2nd IEEE International Conference on Information Management and Engineering pp. 115–117 (2010), http://ieeexplore.ieee.org/lpdocs/epic03/wrapper.htm?arnumber=5477432
14. LeCun, Y., Bengio, Y., Hinton, G.: Deep learning. Nature 521, 436–444 (May 2015)
15. Li, C., Ben Hamza, A.: A multiresolution descriptor for deformable 3d shape retrieval. The Visual Computer 29(6), 513–524 (Jun 2013), https://doi.org/10.1007/s00371-013-0815-3

16. Limberger, F.A., Wilson, R.C.: Feature encoding of spectral signatures for 3d non-rigid shape retrieval. In: British Machine Vision Conf. pp. 1–13
17. Litjens, G.J.S., Kooi, T., Bejnordi, B.E., Setio, A.A.A., Ciompi, F., Ghafoorian, M., van der Laak, J.A.W.M., van Ginneken, B., Sánchez, C.I.: A survey on deep learning in medical image analysis. CoRR abs/1702.05747 (2017), http://arxiv.org/abs/1702.05747
18. Mäenpää, T., Viertola, J., Pietikäinen, M.: Optimising colour and texture features for real-time visual inspection. Pattern Analysis & Applications 6(3), 169–175 (2003), http://dx.doi.org/10.1007/s10044-002-0179-1
19. Masoumi, M., Li, C., Hamza, A.B.: A spectral graph wavelet approach for nonrigid 3d shape retrieval. Pattern Recognition Letters 83, 339–348 (2016), http://www.sciencedirect.com/science/article/pii/S0167865516300617
20. Moore, S., Bowden, R.: Local binary patterns for multi-view facial expression recognition. Computer Vision and Image Understanding 115, 541–558 (2011)
21. Ojala, T., Pietikainen, M., Maenpaa, T.: Multiresolution gray-scale and rotation invariant texture classification with local binary patterns. IEEE Transactions on Pattern Analysis and Machine Intelligence 24(7), 971–987 (jul 2002), http://ieeexplore.ieee.org/document/1017623/
22. Ojala, T., Pietikäinen, M., Harwood, D.: A comparative study of texture measures with classification based on featured distributions. Pattern Recognition 29(1), 51–59 (jan 1996), http://linkinghub.elsevier.com/retrieve/pii/0031320395000674
23. Othmani, A., Voon, L.F.L.Y., Stolz, C., Piboule, A.: Single tree species classification from terrestrial laser scanning data for forest inventory. Pattern Recognition Letters 34(16), 2144–2150 (2013), http://www.sciencedirect.com/science/article/pii/S0167865513002997
24. Shan, C., Gong, S., McOwan, P.: Facial expression recognition based on local binary patterns: A comprehensive study. Image and Vision Computing 27(6), 803 – 816 (2009), http://www.sciencedirect.com/science/article/pii/S0262885608001844
25. Sipiran, I., Lokoc, J., Bustos, B., Skopal, T.: Scalable 3d shape retrieval using local features and the signature quadratic form distance. The Visual Computer (Aug 2016), https://doi.org/10.1007/s00371-016-1301-5
26. Sze, V., Chen, Y., Yang, T., Emer, J.S.: Efficient processing of deep neural networks: A tutorial and survey. CoRR abs/1703.09039 (2017), http://arxiv.org/abs/1703.09039
27. Tangelder, J.W., Veltkamp, R.C.: A survey of content based 3d shape retrieval methods. Multimedia Tools and Applications 39(3), 441–471 (Sep 2008), http://dx.doi.org/10.1007/s11042-007-0181-0
28. Tortorici, C., Werghi, N., Berretti, S.: Boosting 3D LBP-based face recognition by fusing shape and texture descriptors on the mesh. In: 2015 IEEE International Conference on Image Processing (ICIP). pp. 2670–2674. IEEE (sep 2015), http://ieeexplore.ieee.org/document/7351287/
29. Wang, P., Li1, W., Ogunbona, P.O., Wan, J., Escalera, S.: Rgb-d-based motion recognition with deep learning: A survey. Int. Journal of Computer Vision (to appear 2017)
30. Wang, X., Mirmehdi, M.: Archive Film Restoration Based on Spatiotemporal Random Walks, pp. 478–491. Springer Berlin Heidelberg, Berlin, Heidelberg (2010), http://dx.doi.org/10.1007/978-3-642-15555-0_35
31. Werghi, N., Berretti, S., Bimbo, A., Pala, P.: The mesh-lbp: computing local binary patterns on discrete manifolds. In: Proceedings of the IEEE International Conference on Computer Vision Workshops. pp. 562–569 (2013)
32. Werghi, N., Berretti, S., Del Bimbo, A.: The mesh-lbp: a framework for extracting local binary patterns from discrete manifolds. IEEE Transactions on Image Processing 24(1), 220–235 (2015)

33. Werghi, N., Rahayem, M., Kjellander, J.: An ordered topological representation of 3d triangular mesh facial surface: concept and applications. EURASIP Journal on Advances in Signal Processing 2012(1), 144 (2012)
34. Werghi, N., Tortorici, C., Berretti, S., del Bimbo, A.: Local binary patterns on triangular meshes: Concept and applications. Computer Vision and Image Understanding 139, 161–177 (oct 2015), http://linkinghub.elsevier.com/retrieve/pii/S1077314215000843
35. Werghi, N., Tortorici, C., Berretti, S., Del Bimbo, A.: Computing local binary patterns on mesh manifolds for 3D texture retrieval. Proceedings of the 2015 Eurographics Workshop on 3D Object Retrieval pp. 91–94 (2015)
36. Werghi, N., Tortorici, C., Berretti, S., Del Bimbo, A.: Representing 3D texture on mesh manifolds for retrieval and recognition applications. In: 2015 IEEE Conference on Computer Vision and Pattern Recognition (CVPR). vol. 07-12-June, pp. 2521–2530. IEEE (jun 2015), http://ieeexplore.ieee.org/document/7298867/
37. Werghi, N., Tortorici, C., Berretti, S., Del Bimbo, A.: Boosting 3D LBP-Based Face Recognition by Fusing Shape and Texture Descriptors on the Mesh. IEEE Transactions on Information Forensics and Security 11(5), 964–979 (may 2016), http://ieeexplore.ieee.org/document/7373633/
38. Wu, X., Sun, J.: An Effective Texture Spectrum Descriptor. In: 2009 Fifth International Conference on Information Assurance and Security. vol. 2, pp. 361–364. IEEE (2009), http://ieeexplore.ieee.org/document/5283492/
39. Zeppelzauer, M., Poier, G., Seidl, M., Reinbacher, C., Schulter, S., Breiteneder, C., Bischof, H.: Interactive 3d segmentation of rock-art by enhanced depth maps and gradient preserving regularization. J. Comput. Cult. Herit. 9(4), 19:1–19:30 (Sep 2016), http://doi.acm.org/10.1145/2950062
40. Zhenhua Guo, Lei Zhang, Zhang, D.: A Completed Modeling of Local Binary Pattern Operator for Texture Classification. IEEE Transactions on Image Processing 19(6), 1657–1663 (jun 2010), http://ieeexplore.ieee.org/document/5427137/